SUPPLEMENTARY INFORMATION

Electrokinetic elucidation of the interactions between persistent luminescence nanoprobes and the binary Apolipoprotein-E /Albumin protein system

Gonzalo Ramírez-García,[a,b,c] Fanny d'Orlyé,[b] Cyrille Richard,[c] Nathalie Mignet,[c] Anne Varenne[b]*

[a] Centro de Física Aplicada y Tecnología Avanzada, Universidad Nacional Autónoma de México. 3001, Blvd. Juriquilla, 76230, Querétaro, México.

[b] Chimie ParisTech, PSL University, CNRS 2027, Institute of Chemistry for Life and Health Sciences, 75005, Paris, France.

[c] Université de Paris, CNRS, INSERM, UTCBS: Chemical and Biological Technologies for Health, Faculté de Pharmacie, 75006, Paris, France.

*Corresponding author. E-mail: anne.varenne@chimieparistech.psl.eu

Experimental protocols used for the synthesis, functionalization and characterization of ZGO-PEG

Materials and reagents

Gallium oxide and chromium nitrate were provided from Alfa Aesar chemicals, zinc nitrate from Fluka, and α-methoxy-ω-N-hydroxysuccinimide polyethylene glycol (5000 Da) from Iris Biotech GmbH. (3-aminopropyl)triethoxysilane (APTES) and dimethylformamide (DMF) were purchased from Sigma-Aldrich. Ammonium carbonate buffer pH 7.4 (ACB) was prepared in an initial ionic strength of 50 mM by dissolving the proper amounts of ammonium carbonate and ammonium bicarbonate (Sigma-Aldrich). The ACB solution was sonicated and then filtered through a 0.2 µm nylon syringe filter (Corning, NY, USA) before use. The human Apolipoprotein-E (ApoE) was carefully diluted in ACB pH 7.4 (the same buffer solution in which was supplied by Merck Millipore) at the different ionic strengths analyzed in this work. Human serum albumin (HSA) was bought from LFB Biotechnologies (France) and similarly dissolved in ACB.

Synthesis and characterization of the PEGylated $ZnGa_{1.995}Cr_{0.005}O_4$ persistent luminescent NPs

$ZnGa_{1.995}Cr_{0.005}O_4$ nanoparticles were prepared using the hydrothermal synthesis process described by *C. Richard et al.*[1] Briefly, 8.94 mmol of gallium oxide were mixed with concentrated nitric acid (35 wt %), and reacted in a Teflon-lined stainless-steel autoclave at 150 °C overnight to form gallium nitrate. 0.04 mmol of chromium nitrate and 8.97 mmol of zinc nitrate in 10 mL of water were added to the previous mixture under vigorous stirring. Then, 7.5 mL of ammonium hydroxide solution (30 wt %) were added until gelation at pH 7.5. The resulting dispersion was stirred for 3 hours at room temperature, transferred into a 25 mL teflon-lined stainless-steel autoclave, and heated for 24 hours at 120 °C. The product of the reaction was washed three times with water and ethanol, and then oven-dried at 60 °C for 2 hours. The powder was finally sintered in an air atmosphere at 750 °C for 5 hours, crushed and re-suspended in 5.0 mM NaOH

solution, and vigorously stirred overnight. The resulted hydroxylated material (ZGO-OH) was fractioned by repeated centrifugation steeps, and then collected the 90 nm NP fraction (hydrodynamic diameter) considering a PDI lower than 0.1. Aminosilane-functionalized nanoparticles (ZGO-NH_2) were obtained by adding 20 µL of APTES to a suspension of 5.0 mg ZGO-OH dispersed in 2.0 mL DMF. The reaction mixtures were sonicated for the first 2 minutes using a Branson Ultrasonic Cleaner 1210, and kept under vigorous stirring for 5 hours at room temperature in a glass balloon flask. Particles were washed from the unreacted APTES by three centrifugation and redispersion steps in DMF. The resulting ZGO-NH_2 were reacted overnight at 90 °C with 10 µmol α-Methoxy-ω-N-hydroxysuccinimide polyethylene glycol (5000 Da) in 1.0 mL DMF. The resulting ZGO-PEG were washed three times in water and re-dispersed in ACB at the corresponding ionic strength (IS).

For characterization, Transmission Electron Microscopy (TEM) images were obtained using a JEOL JEM-1010 microscope equipped with an ORIUS digital camera, by GATAN. The FTIR-ATR spectra of the dehydrated NPs were recorded with a Perkin-Elmer 100 spectrometer. Nanoparticle hydrodynamic size and ζ-potential were determined in ACB at 30 mM by dynamic light scattering (DLS) and laser Doppler electrophoresis (LDE) measurements, respectively with Nano ZS Zetasizer instrument (Malvern Instruments, France).

Statistical Analysis

Each analysis in this work was performed four times to obtain representative values. Binding curves were analyzed using Graphpad Prism Version 5.00 curve-fitting software for nonlinear regression (Graphpad Software, San Diego, CA). The mean differences between multiple groups were determined by one-way ANOVA, followed by the Tukey multiple comparison test with an α level of 0.05. The version 8 of JMP software from SAS was used.

Physicochemical characterization of the PEG-functionalized persistent luminescence nanoparticles

This section describes the details of characterization presented in Figure 1 of the main manuscript. The NPs with optimized formula $ZnGa_{1.995}Cr_{0.005}O_4$ (ZGO-NPs) were synthesized in the form of a fine white powder. Afterward, a three steps functionalization sequence was set up to obtain the PEG-modified NPs (Figure 1-A). First, the hydroxylation process in 5.0 mM NaOH allows obtaining ZGO-OH, in which the hydroxyl groups induce electrostatic repulsions, preventing aggregation when dispersed in aqueous solutions. The subsequent modification corresponds to the covalent bond of APTES at the ZGO-OH surface, which is derived from the reaction between the hydroxyl groups at the NPs surface and the siloxane moieties (-Si-O-Si-) resulting from the partial hydrolysis of the alkoxysilane molecules in anhydrous conditions. Finally, an inert hydrophilic molecular layer of PEG was incorporated at the nanoparticle surface. The PEG molecules were covalently linked to the ZGO-NH_2 via an amide bond between the primary amino group of APTES and the N-hydroxysuccinimide activated 5 kDa polyethylene glycol to give stealth ZGO–PEG.

The particle size and morphology of ZGO-PEG were analyzed via TEM (Figure 1-B). An average solid diameter of 30 nm with semi-spherical shape was observed, and the particle size distribution is shown in the inset histogram. The success of the reactions involved in the formation of the PEGylated NPs was confirmed by the Fourier transform infrared spectroscopy (FTIR) spectra (Figure 1-C). A broad band corresponding to the O-H bonds vibration is observed around 3309 cm^{-1}. This signal is characteristic of hydrated systems and confirms the activation of the nanoparticles during the first functionalization step to produce ZGO-OH. Upon modification with APTES (ZGO-NH_2), two bands were observed at 3516 and 3475 cm^{-1}, that can be ascribed to primary amine N-H bonds. The band at 1814 cm^{-1} is attributed to the C-N

stretching vibration. The peaks at 2976 and 2901 cm^{-1} are attributed to the asymmetric and symmetric stretching vibrations, respectively, of the CH_2 moiety in the aminopropyl chains. Likewise, the stretching vibrations of the siloxane (Si–O–Si) and the bending vibrations of the silanol (Si–O–H) are observed at around 1374 and 1103 cm^{-1}, respectively, thus verifying the coupling of APTES. For the ZGO-PEG, the intensity of the bands at 2976 and 2901 cm^{-1} was increased due to the incorporation of the 5kD polyethylene glycol, while the bands corresponding to the amino groups were no longer observed. The band detected at 1647 cm^{-1} was attributed to the C=O stretching vibration in the amide group, and the bending frequencies for asymmetric and symmetric $–CH_3$ were observed at 1394 and 1249 cm^{-1}, respectively. The most intense signal was observed at 1067 cm^{-1}, corresponding to the C-O stretching in the repeated ethylene glycol section. A detailed characterization of the colloidal properties of these NPs in physiologically relevant media are described in our previously reported article[2], indicating a preserved colloidal stability of the ZGO-PEG above all the range of conditions used in the present work. All these observations corroborate the successful functionalization of the ZGO-NPs with the PEG chains.

As an additional control, the viscosity and conductivity of the BGE containing proteins were evaluated throughout the range of protein concentrations and mixtures (Figures S1 and S2, respectively). Since no significant variation in viscosity ($89 \pm 7 \times 10^{-5}$ Pa.s) or conductivity ($372 \pm 8 \times 10^{-3}$ $S.m^{-1}$) was observed under the experimental conditions, the variations in the electrophoretic profiles can be exclusively attributed to the interactions between ZGO-PEG and HSA, ApoE, or their mixtures.

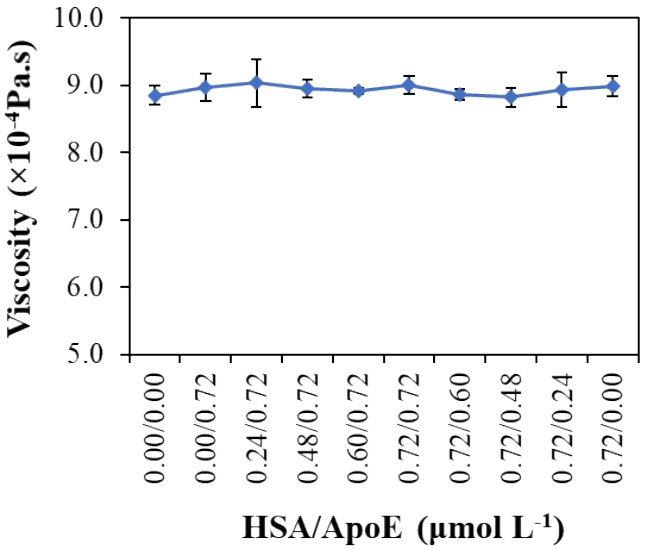

Figure S1. Analysis of the viscosity as a function of the HSA/ApoE molar ratio in 15 mM ACB (pH 7.4). T= 37 °C.

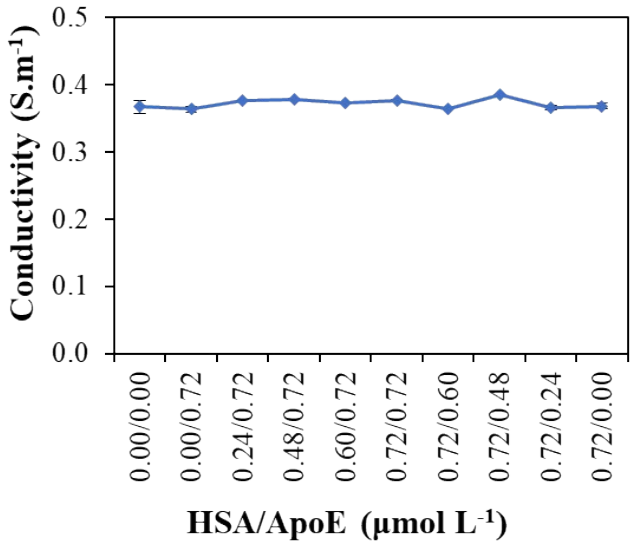

Figure S2. Analysis of the conductivity as a function of the HSA/ApoE molar ratio in 15 mM ACB (pH 7.4). T= 37 °C.

Equations for determination of interactions according HDCE and ACE models

For interactions with HSA, the vacancy peaks areas and the external calibration (Figure S3) gave access to the concentration of protein bound to the ZGO-PEG, and therefore to the binding constant and the number of binding sites.

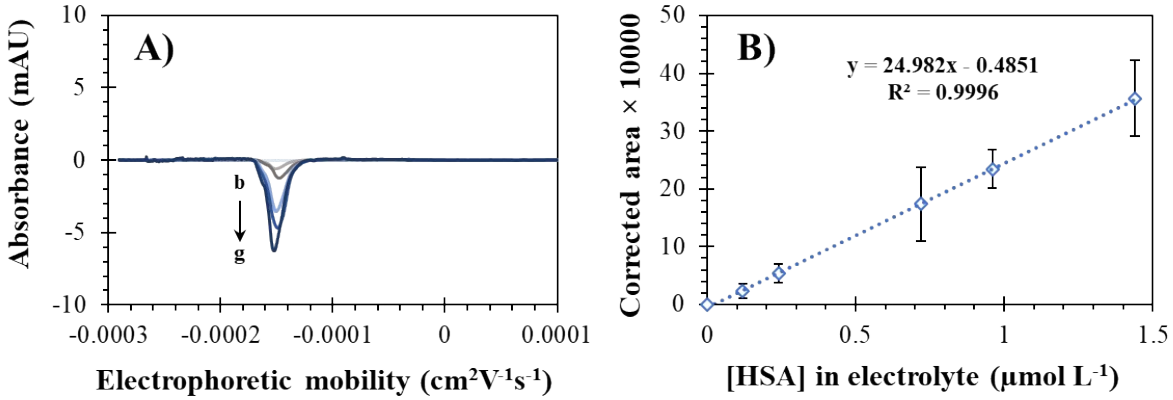

Figure S3. A) Representative electropherograms obtained by the injection of 30 mM ACB (pH 7.4) for the external calibration of HSA according to the Hummel-Dreyer method. The capillary was pre-conditioned with varied protein concentrations: b) 0, c) 0.12, d) 0.24, e) 0.72, f) 0.96, g) 1.44 µM. The separation was performed with E=14 kV, and the signals obtained with a UV-Vis detector (λ = 200 nm). B) Corresponding calibration curve.

As reported in our previous work [3], the vacancy peak area increased linearly with the ligand concentration (HSA) in the BGE. The fraction "r" describing the ratio of bound proteins $[L]_b$ to total NPs $[S]_t$ can be determined by varying the amount of protein present in the BGE during the separation [3,4]. $[S]_t$ was fixed in the experimental conditions at 0.2

mg.mL^{-1}. When the HDCE approach was applied (ZGO-PEG/HSA interactions), the bound protein concentrations [L]b could be obtained employing equation 1:

$$[L]_b = \frac{A_{NP} - A_c}{A_c}[L]_t \qquad \text{Eq.1}$$

where A_c is the resulting negative or vacancy peak area of the standard calibration (obtained by the BGE injection into the pre-filled capillary with varied protein concentrations $[L]_t$), and ANP is the negative peak area arising from the injection of the NP sample. The fraction *r* can be defined in terms of the association constant *Ka* to obtain the binding parameters for the ZGO-PEG/HSA nanocomplex:

$$r = \frac{[L]_b}{[S]_t} = n\frac{[L].K_a}{[L].K_a + 1} \qquad \text{Eq.2}$$

The value "*r*" could vary from *0* to *n*. The parameter *r* obtained at different protein concentrations was adequately fitted to a hyperbolic binding isotherm using nonlinear regression (Figure S4-A). Equation 2 can be linearized as follows:

$$\frac{r}{[L]} = -K_a r + K_a n \qquad \text{Eq.3}$$

When plotting *r*/[L] versus *r*, the *Scatchard's plot* is obtained, and it allows the determination of K_a (slope in absolute value) and n (x-intercept) (See Figure S4-B).

Otherwise, when the ACE approach was applied (ZGO-PEG/ApoE interactions), the fraction "*v*" could be defined as the ratio of the bound NPs $[S]_b$ to total NPs [S]t. [S]t is fixed in the experimental conditions at 0.2 mg.mL^{-1}. The fraction *v* was calculated from the variations in the migration time of the ZGO-PEG/APoE complex according to the different ApoE concentrations in the BGE. Equation 4 describes this ratio [5,6].

$$v = \frac{[S]_b}{[S]_t} = \frac{\mu_L - \mu_0}{\mu_{max} - \mu_0} \qquad \text{Eq.4}$$

where μ_L is the observed electrophoretic mobility of the nanocomplex at a given protein concentration [L], μ_0 the electrophoretic mobility of the NPs in free protein-BGE, and μ_{max} the maximal electrophoretic mobility reached under saturation conditions. The parameter *v* obtained at different protein concentrations was also fitted to a hyperbolic binding isotherm using nonlinear regression (Figure S4-C).

In order to calculate the binding parameters describing the nanocomplex ZGO-PEG/ApoE, a system in which the protein L bound to multiple independent binding sites in the nanoparticle surface was assumed. Here, the variable for association v could be also defined as the fractional saturation of the nanoparticles [6]:

$$\nu = \frac{[S]_b}{[S]_t} = \frac{[L]^n}{[L]^n + K_d} \qquad \text{Eq.5}$$

where K_d is the microscopic dissociation equilibrium constant (the inverse value of K_a). Rearranging the equation 5 into a linear form [7], the *Hill's equation* is obtained:

$$log\left[\frac{\nu}{(1-\nu)}\right] = nlog[L] - logK_d \qquad \text{Eq. 6}$$

The plot of log [L] versus log [*v*/ (1-*v*)] is known as the Hill's plot, and it is presented in Figure S4-D. Based on Equation 6, the Hill's plot should have a slope n. However, the experimentally determined slope does not reflect the number of binding sites. The slope of a Hill's plot is therefore denoted by "n_H" (the Hill's coefficient), which measures the degree of binding cooperativity. The values of n_H >1 and n_H <1, represents positive and negative cooperativity, respectively, while n_H =1 means non-cooperativity.[8]

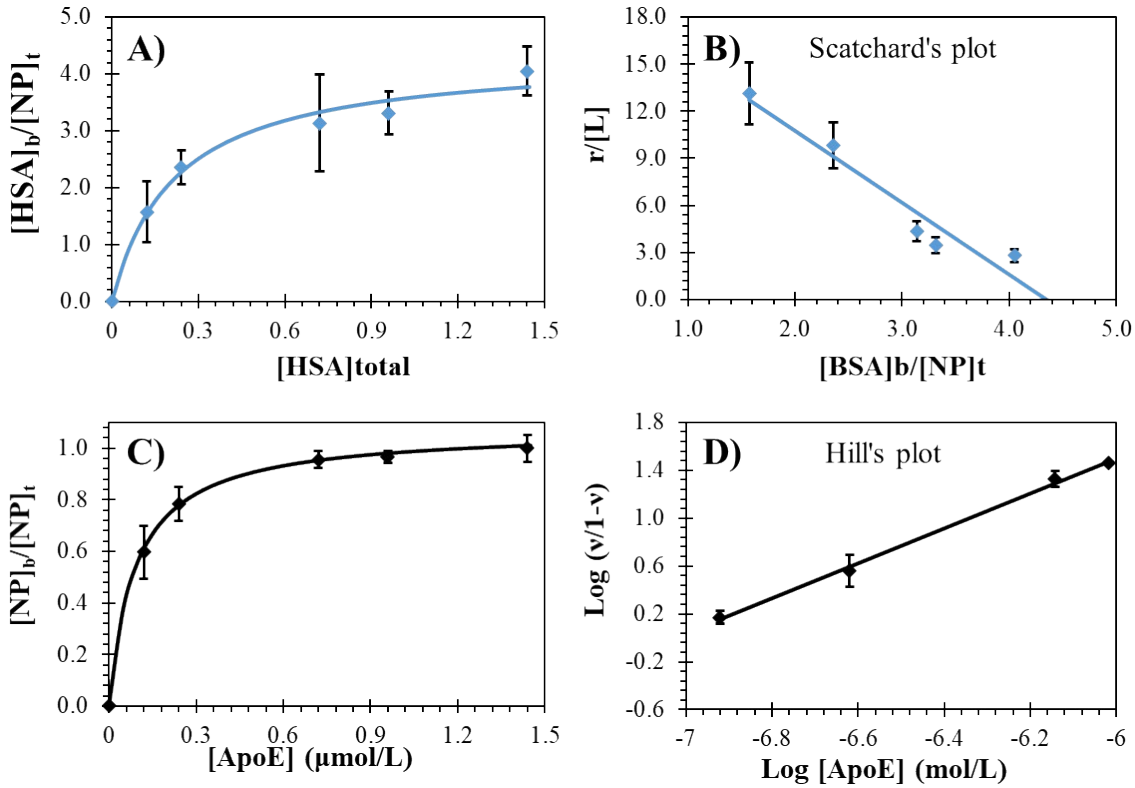

Figure S4. A) Model fitting curves for ZGO-PEG interactions with HSA, and B) corresponding Scatchard's plot. C) Model fitting curves for ZGO-PEG interactions with ApoE, and D) corresponding Hill's plot. BGE: ACB (pH 7.4) at 30 mM ionic strength. Error bars indicate the ± standard deviation of four sets of samples prepared by separate at each protein concentration.

Pre-incubation effects on the interactions between ZGO-PEG and a mixture of HSA and ApoE proteins

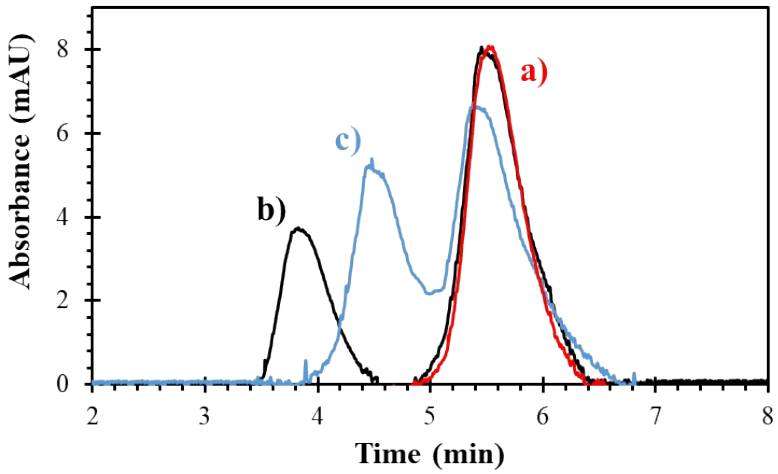

Figure S5. Set of representative electropherograms obtained at λ = 200 nm for analysis of the competitive interactions. The electropherograms are identified according to the BGE composition (BGE) and pre-incubated sample (S): a) BGE=ACB, S=HSA, b) BGE=ACB, S=ZGO-PEG/HSA, c) BGE=ACB+ApoE, S=ZGO-PEG/HSA. Protein concentration was 1.44 µM for all cases. Initial BGE was 30 mM ACB (pH 7.4). E=12.0 kV.

References

1 T. Maldiney, A. Bessière, J. Seguin, E. Teston, S. K. Sharma, B. Viana, A. J. J. Bos, P. Dorenbos, M. Bessodes, D. Gourier, D. Scherman and C. Richard, *Nat. Mater.*, 2014, **13**, 418–426.

2 G. Ramírez-García, F. d'Orlyé, S. Gutiérrez-Granados, M. Martínez-Alfaro, N. Mignet, C. Richard and A. Varenne, *Colloids Surfaces B Biointerfaces*, 2015, **136**, 272–281.

3 G. Ramírez-García, F. d'Orlyé, S. Gutiérrez-Granados, M. Martínez-Alfaro, N. Mignet, C. Richard and A. Varenne, *Colloids Surfaces B Biointerfaces*, 2017, **159**, 437–444.

4 W. Yan and C. L. Colyer, *J. Chromatogr. A*, 2006, **1135**, 115–121.

5 N. Li, S. Zeng, L. He and W. Zhong, *Anal. Chem.*, 2010, **82**, 7460–7466.

6 S. P. Boulos, T. A. Davis, J. A. Yang, S. E. Lohse, A. M. Alkilany, L. A. Holland and C. J. Murphy, *Langmuir*, 2013, **29**, 14984–14996.

7 J. N. Weiss, *FASEB J.*, 1997, **11**, 835–841.

8 M. Matczuk, K. Anecka, F. Scaletti, L. Messori, B. K. Keppler, A. R. Timerbaev and M. Jarosz, *Metallomics*,

2015, **7**, 1364–1370.